DIAGNOSTYKA, 2026, Vol. 27, No. 3

e-ISSN 2449-5220
DOI: 10.29354/diag/226162

DIGITAL TWIN IMPLEMENTATION FOR CONDITION MONITORING OF A COLLABORATIVE ROBOT

Iwona Monika KOMORSKA [*], **Grzegorz STEFANIAK**

Faculty of Mechanical Engineering, Casimir Pulaski Radom University, Poland
[*] Corresponding author, e-mail: iwona.komorska@urad.edu.pl

Abstract

The article presents the implementation and experimental verification of a Digital Twin framework for sensorless condition monitoring, understood as monitoring without the need for additional, non-native sensing hardware, of a Universal Robots UR3e collaborative robot. The system combines real-time data acquisition via the RTDE interface with a virtual reference model estimating nominal motor-current behaviour during repeatable motion cycles. The anomaly detection criterion is based on residuals between measured and predicted current signals, enabling the distinction between process disturbances and mechanical degradation. Validation on a CP-Factory workstation using a figure-eight trajectory, induced resistance and simulated payload loss shows sensitivity to low-amplitude anomalies and allows separation of friction increase, joint resistance and payload loss.

Keywords: Digital Twin, collaborative robot, UR3e, motor current signature analysis, anomaly detection, predictive maintenance

1. INTRODUCTION

The reliability of robotic systems has become one of the key determinants of manufacturing efficiency. In highly automated production cells, unplanned downtime affects not only the availability of a single robot, but also the continuity of upstream and downstream operations [1]. For this reason, maintenance strategies are shifting from reactive repair and scheduled replacement towards condition monitoring and predictive maintenance, where early symptoms of degradation are detected before they reach a level that triggers production stoppage.

Collaborative robots create a particular diagnostic challenge. Their safety systems are designed primarily to protect humans and the workstation and therefore react to events that exceed defined safety limits. The current safety framework for industrial robots is described by ISO 10218-1:2025 [2], while collaborative applications are still commonly discussed with reference to ISO/TS 15066:2016 [3]. These documents are essential for risk reduction, but they do not by themselves provide early-stage mechanical diagnosis. Phenomena such as grease degradation, bearing defects, backlash increase, harmonic-drive wear or local friction changes can reduce repeatability and process quality long before the robot enters a protective stop.

Digital Twin technology provides a way to close this gap [3]. A Digital Twin differs from a Digital Shadow because it is not limited to one-way state visualization; it enables a closed comparison between the physical asset and a virtual reference model, and can support recalibration, simulation and "what-if" analysis [5-7]. In manufacturing applications, this architecture is formalized by the ISO 23247 framework [8] and is also compatible with the broader IoT reference architecture defined in ISO/IEC 30141:2024 [9]. Recent studies show that digital twins are increasingly used not only for visualization and programming, but also for self-learning decision-making, status monitoring and fault diagnosis of industrial robots [10-13].

The state of the art in robot diagnostics shows that the most critical mechanical components are speed reducers, bearings and drive units. Comprehensive reviews of industrial robot diagnostics and manipulator faults indicate that reducers can account for approximately 50-60% of mechanical failures, bearings for 20-30%, and electromechanical components for a smaller but still significant share [14-16]. In lightweight collaborative robots, harmonic drives are particularly critical, given that their thin flexsplines provide compactness and low backlash, but are sensitive to fatigue, pitting, friction changes and lubrication degradation. Diagnosisrent-based diagnosis of harmonic drives under time-varying speed has recently been demonstrated by Zhang et al. [17], while harmonic-drive and RV-reducer

Received 2026-05-21; Accepted 2026-08-10; Available online 2026-08-17

diagnosis has also been studied using multi-sensor fusion, sound-vibration spectrograms, transfer learning and RUL prediction [18-22].

The literature also confirms that bearing defects, backlash and friction changes can be detected from vibration or current signals. Rolling-element defects in multi-joint robots have been analysed using dynamic modelling and deep learning [23]. RV reducer diagnosis has been addressed using PHM-oriented electrical signal analysis and EEMD-based feature extraction [24,25]. Earlier experimental studies on industrial robot joints showed that discrete wavelet transform combined with neural networks can detect bearing faults and backlash in robot transmissions [26,27]. More recent work has extended this direction towards real-time multi-joint diagnosis using DWT and Slantlet transforms [28].

Digital twins are particularly useful when real fault data is scarce. Reducer faults and manipulator faults are expensive and risky to reproduce on a production robot, so virtual models can generate controlled fault scenarios and support machine-learning models. Recent works combine digital twins with deep learning for reducers [22], domain adaptation for digital-twin-supported fault diagnosis [29], and GRU-based diagnosis of industrial robots [30]. These studies indicate that a major open problem is the sim-to-real gap: a model trained only on simulated data may not generalize well to the physical robot unless it is calibrated or adapted using measured signals.

In this study, a Digital Twin of a UR3e collaborative robot is used as an active diagnostic observer. The proposed approach does not require additional joint-mounted vibration sensors. Instead, it uses motor-current signals acquired from the robot controller and compares them with the nominal behaviour predicted by the virtual model. The diagnostic assumption is that increased resistance, local friction growth, backlash effects and payload disturbances produce characteristic residual patterns. Unlike standard safety systems, which are designed to stop dangerous motion, the proposed framework aims to detect low-amplitude deviations that may indicate early degradation or process errors.

The contribution of this paper is threefold. First, it implements a real-time Digital Twin architecture for the UR3e robot using RTDE data exchange and a calibrated reference model. Second, it analyses motor-current residuals as a sensorless diagnostic signal for increased motion resistance and payload loss. Third, it introduces a practical interpretation layer in which positive residuals indicate increased energetic demand, whereas negative residuals indicate a reduction in expected load, such as loss of a transported object. The experimental results are discussed with reference to the figures showing the workstation, model architecture, kinematic synchronization and current-residual responses.

2. DIGITAL TWIN ARCHITECTURE AND MODELLING METHODOLOGY

2.1. Physical and virtual world integration

The proposed system follows the distinction between a digital model, a Digital Shadow and a Digital Twin. A digital model is a static virtual representation without automatic data exchange. A Digital Shadow receives data from the physical object but does not actively influence or recalibrate the reference model. A Digital Twin, in contrast, operates as a bidirectionally synchronized system in which measured data and model-based predictions are continuously compared [5-7].

In this research, the Digital Twin acts as an active observer of the UR3e robot. Its role is to separate normal dynamic effects, such as gravity and velocity-dependent friction, from deviations caused by process errors or mechanical degradation. The architecture follows the ISO 23247 terminology [8]. The Observable Manufacturing Element is the physical UR3e robot with its gripper and payload. The Device Communication Entity is the RTDE communication layer. The Digital Twin Entity contains the virtual kinematic, dynamic and diagnostic models. The User Entity is responsible for visualization, reporting and operator interaction. This separation is crucial as it ensures that the decision logic for residual generation belongs to the Digital Twin Entity, whereas the operator interface belongs to the User Entity.

2.2. Technical specification of the UR3e cobot

The UR3e is a compact six-degree-of-freedom collaborative manipulator designed for precise light-duty tasks such as assembly, dispensing, inspection and small-part handling [31]. It belongs to the Universal Robots e-Series and is characterized by a nominal payload of 3 kg, a reach of 500 mm and a low structural mass, which makes it suitable for laboratory and flexible production stations. The laboratory workstation with the UR3e is shown in Fig. 1, while Fig. 2 presents the joint-axis layout used for the kinematic description. As illustrated in these figures, the diagnostic interpretation of current residuals depends on the spatial configuration of the robot: gravitational loading, joint orientation and the sign of joint motion determine whether a fault amplifies or attenuates the measured current.

The manipulator has a serial 6R kinematic structure composed of the Base, Shoulder, Elbow, Wrist 1, Wrist 2 and Wrist 3 joints. Each joint is implemented as an integrated mechatronic drive module containing a permanent-magnet synchronous motor, an electromagnetic brake, an encoder system, a compact reduction transmission and local drive electronics. In the UR3e class, the drive units are designed to combine high positioning repeatability with the low inertia required for collaborative operation. The final wrist joint can rotate continuously, which is useful in screwing, polishing and dispensing tasks, but also creates specific diagnostic requirements because cable routing, repetitive wrist motion and small nominal torques can make wrist-axis residuals more sensitive to disturbances.

Fig. 1. CP-Factory workstation with a UR3e collaborative robot in the laboratory

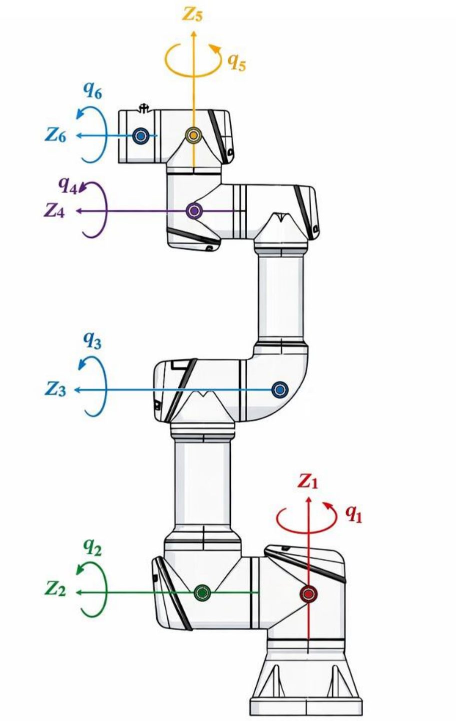

Fig. 2. Diagram of joint axes and joint variables of the UR3e robot

The UR3e contains several internal sensor channels that are relevant for condition monitoring. The absolute encoder system provides joint position feedback used by the controller and by the Digital Twin for kinematic synchronization. Joint velocities can be obtained directly from the controller stream or derived from encoder trajectories after filtering. Motor-current signals, available from the drive system, are used in this work as a sensorless proxy for generated joint torque. Digital and analog I/O channels provide information about the state of peripheral devices, such as the vacuum gripper, and are useful for interpreting process faults, for example payload loss.

An important element of the e-Series hardware is the integrated six-axis force-torque sensor mounted at the tool flange. It measures forces and torques acting at the end effector and is used by the robot controller for force-limited operation, contact detection and collaborative safety functions. In this study, the main diagnostic path is based on motor-current residuals, but the force-torque sensor remains an important contextual source of information. It can support the interpretation of contact events, distinguish external interaction from internal drive resistance and reduce ambiguity in cases where the sign of the current residual alone is insufficient.

From the communication perspective, the robot provides access to joint positions, velocities, motor currents, tool data, I/O states and selected controller variables through the RTDE interface. Recent work on UR RTDE communication confirms that this interface is suitable for high-frequency acquisition and control-oriented integration [32]. In the present implementation, the RTDE stream supplies Digital Twin with proprioceptive data required for inverse-dynamics estimation and residual analysis. The use of controller-internal signals makes the proposed approach practically attractive, because no additional accelerometers or external current probes are required during the baseline experiment.

Table 1 summarizes the key UR3e parameters used in the model. The pose repeatability specified according to ISO 9283 [33] is important for the proposed method because small backlash- or friction-related deviations can only be interpreted reliably when the nominal repeatability of the robot is known.

Table 1. Technical specifications of the UR3e robot

Parameter	
Payload	3 kg
Reach	500 mm
Weight	11.2 kg
Pose repeatability	±0.03 mm
System frequency	500 Hz
Typical power	100 – 150 W
Cleanroom	ISO Class 5
IP classification	IP54

2.3. Mechanical model and current residuals

The analytical basis of the Digital Twin is a rigid-body model of the manipulator [34]. The robot is represented as an open kinematic chain, with each link described by mass, inertia tensor and centre-of-mass coordinates. This description is sufficient to reproduce the main dynamic effects that influence the motor-current demand during repeatable robot motion: inertia, gravity, velocity-dependent effects and joint friction. In the proposed condition monitoring framework, the model is not used only for visualization, but also as a reference system generating the nominal response expected from a healthy robot. The general joint-space dynamics can be expressed as:

$$\tau_{model} = M(q)\ddot{q} + C(q,\dot{q})\dot{q} + G(q) + F(\dot{q}) + \tau_{ext} \quad (1)$$

where $M(q)$ denotes the inertia matrix, $C(q,\dot{q})\dot{q}$ represents the Coriolis and centrifugal forces, $G(q)$ is the gravity vector, and $F(\dot{q})$ defines the friction model.

The term τ_{ext} plays a key role in the diagnostic architecture, representing external interactions (collisions or changes in payload mass) that the system is intended to identify. As indicated by Thomsen and Rasmussen [23], precise identification of link inertia tensors and centers of mass is essential to mitigate the so-called Sim-to-Real gap, which in this work was achieved through numerical calibration of the model with respect to the nominal motor currents of the real machine.

Friction modelling is essential because harmonic-drive and reducer faults often manifest as changes in resistive torque before a visible positioning error occurs [17,18,35]. The implemented friction layer includes viscous and Coulomb components:

$$\tau_{f,i} = f_{v,i}\dot{q} + f_{c,i} \cdot sgn(\dot{q}_i) \quad (2)$$

where:

$\tau_{f,i}$ – the friction torque generated at the i-th joint of the manipulator.

$f_{v,i}$ – the viscous friction coefficient, which determines resistance proportional to the motion velocity.

$\dot{q}_i$ – the angular velocity of the i-th joint, obtained from encoders or computed based on the prescribed trajectory.

$f_{c,i}$ – the Coulomb (static/dry) friction coefficient, representing a constant resistance independent of velocity magnitude.

$sgn(\dot{q}_i)$ – the sign (signum) function of the angular velocity, which assumes values of +1 or −1, ensuring that friction always acts in the direction opposite to the motion vector.

The current-to-torque relationship was interpreted using the motor torque constant, gear ratio and mechanical efficiency:

$$\tau_{real} = I_{motor} \cdot k_t \cdot N \cdot \eta \quad (3)$$

where I_{motor} is the RMS motor current, k_t denotes the torque constant, N is the gear ratio (101:1 for the UR3e), and η represents the mechanical efficiency.

The motor torque constant k_t defines how many newton-meters of torque the motor generates per ampere of current (Nm/A). This constant varies depending on the joint size—for the smallest drive units (size 0 in wrist joints J4–J6), it is approximately 0.0945 Nm/A [32]. Angular position q and angular velocity $\dot{q}$ data acquired from encoders serve as control inputs for the virtual model, enabling real-time computation of the residual signal $R(t)$.

The current residual is defined as the difference between the current-related torque demand measured in the real robot and the nominal value predicted by the Digital Twin for the same joint position and motion conditions.

If the residual is positive, it means the robot requires more current than expected, which may indicate increased friction, external resistance, or a collision-like interaction. In contrast, a negative residual suggests that the robot needs less current than expected, which is typical in situations such as a sudden loss of payload. Therefore, the residual is interpreted not only based on its magnitude but also considering its direction (positive or negative), how long it persists, which joint it affects, and at what stage of the motion it occurs.

3. HIGH-FIDELITY MECHANICAL MODEL IN THE SIMSCAPE ENVIRONMENT

3.1. Hybrid model structure

The virtual model was developed in MATLAB/Simscape Multibody as a hybrid structure combining a verified kinematic description of the UR e-Series manipulator with additional physical and anomaly detection layers [36]. The base rigid-body structure was used as the nominal geometric and kinematic reference, while the original contribution consisted of CAD-based workstation modelling, gripper modelling, friction-layer implementation and residual-based fault interpretation.

Figure 3 presents the block architecture of the UR3e model. This diagram illustrates the functional mapping of the Digital Twin, where kinematic inputs from the physical robot feed the virtual model, the model estimates nominal dynamic behaviour, and the anomaly detection layer compares this prediction with measured current signals.

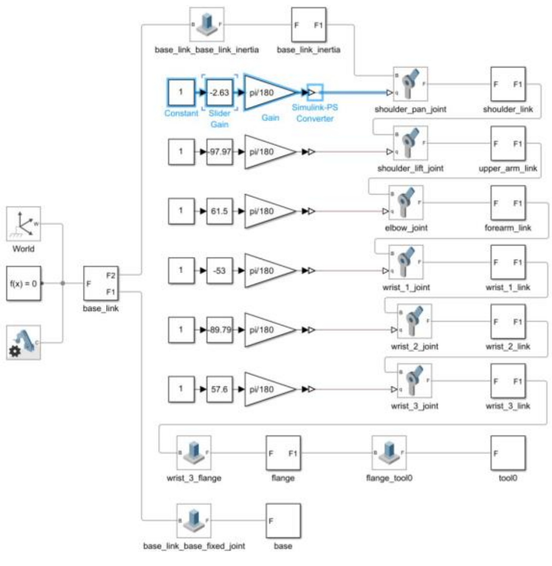

Fig. 3. Block diagram architecture of the UR3e model reflecting the hierarchical structure of the manipulator

3.2. Rigid body tree and inertial parameters

The rigid-body tree structure defines the topology of the manipulator, the link coordinate systems and the inertial parameters required for inverse dynamics [34]. Accurate mass and inertia assignment is crucial because any systematic modelling error appears directly in the residual signal. This is the main source of the sim-to-real gap discussed in digital-twin condition monitoring [29,30].

Figure 4 shows the 3D multibody representation after integration of the geometric and inertial parameters. The geometric fidelity of the model helps verify the correct placement of coordinate frames, joint axes and tool geometry. In diagnostic use, incorrect inertial parameters or tool mass can produce false residuals that resemble payload loss or unexpected contact.

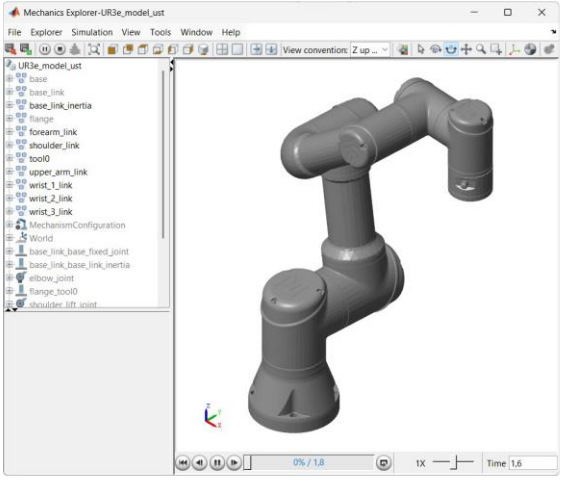

Fig. 4. 3D representation of the multibody model after integration of inertial and geometric parameters

3.3. RTDE communication and synchronization

The RTDE communication layer provides joint positions, velocities and motor-current data from the robot controller. The interface is used to drive the virtual model with the same trajectory executed by the physical or simulated robot. Figure 5 illustrates the signal flow between the communication layer and the dynamic model. The key condition monitoring requirement is temporal consistency: if the measured current and predicted current are shifted in time, residual peaks may be interpreted incorrectly as faults.

The sampling frequency of 500 Hz provides sufficient density for the analysed laboratory trajectories. However, in industrial deployment, timestamping, buffering and packet-loss monitoring should be included because communication jitter may create artificial residuals.

3.4. Validation of the nominal model

The nominal model was validated before fault analysis. The validation trajectory was a figure-eight path, shown in Fig. 6, selected because it excites several joints simultaneously and creates changing gravitational and inertial loads. This trajectory is more informative than a single-axis movement because it reveals coupling effects between joints.

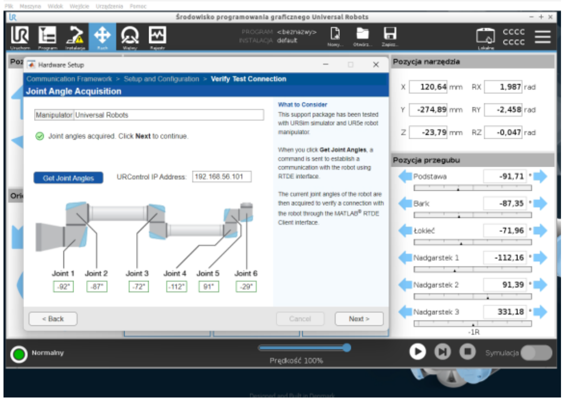

Fig. 5. Signal flow diagram between the communication layer and the dynamic model

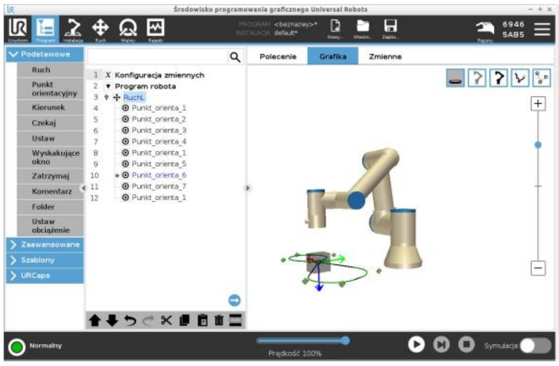

Fig. 6. Robot motion program in the URSim environment used for kinematic validation of the digital model along a figure-eight trajectory

Figure 7 compares the joint-angle trajectories obtained from the URSim/robot data stream and from the Simscape model.

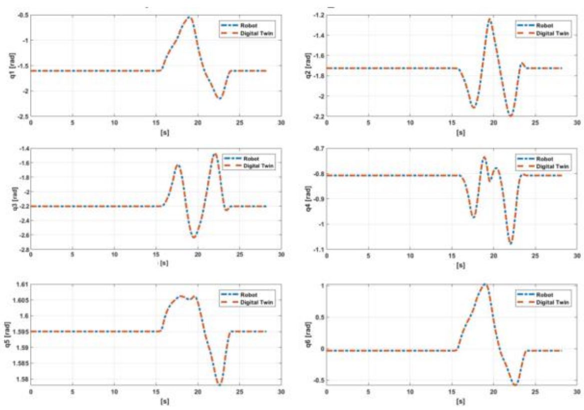

Fig. 7. Comparison of joint angle trajectories obtained from URSim and from the UR3e robot

Although a small-time synchronization delay (phase shift of approximately 0.7 s) is visible in the raw logged signals due to RTDE start-trigger latency, the spatial path tracking is highly accurate. To evaluate this kinematic agreement quantitatively, the trajectory errors were computed both before and after compensating for the phase lag. The results are summarized in Table 2.

Table 2. Kinematic synchronization error metrics (joint angles) between the reference model and the physical robot

Joint	Raw RMSE [rad]	Aligned RMSE [rad]	Raw MAE [rad]	Aligned MAE [rad]
J1	0.08227	0.00130	0.06754	0.00092
J2	0.09503	0.00273	0.08559	0.00237
J3	0.08952	0.00507	0.07626	0.00427
J4	0.05694	0.00094	0.04337	0.00059
J5	0.00610	0.00027	0.00471	0.00020
J6	0.08226	0.00130	0.06750	0.00092

As presented in Table 2, after phase alignment, the Root Mean Square Error (RMSE) for all joints (J1-J6) falls below 0.0051 rad (0.29 deg), and the Mean Absolute Error (MAE) remains below 0.0043 rad. The smallest deviation is observed at joint J5 with an aligned RMSE of 0.00027 rad (0.015 deg). This quantitative agreement confirms the high fidelity of the kinematic synchronization and justifies the use of residual analysis in subsequent diagnostic experiments, ensuring that current anomalies are not artifacts of kinematic modeling errors.

3.5. Neural reference model

In addition to the physical model, a lightweight neural reference model was implemented to predict nominal motor-current consumption from joint positions and velocities. This part of the Digital Twin was introduced to compensate for effects that are difficult to describe accurately using only analytical equations, such as residual friction nonlinearities, drive-controller behaviour and small differences between the nominal multibody model and the real robot. The neural model therefore does not replace the physical model but complements it as a data-driven approximation of the healthy current response.

The input vector was constructed from proprioceptive signals available through the RTDE stream. For each time sample, the model used joint positions and angular velocities of all six axes. Joint positions describe the configuration-dependent gravitational load, whereas angular velocities carry information about viscous friction and motion direction. Before training, the velocity signals were smoothed because numerical differentiation and controller quantization can introduce high-frequency components that are not related to mechanical degradation. A Savitzky-Golay filtering stage was used to preserve the shape of the trajectory while reducing local noise in the derivative estimates.

All input variables were standardised using the Z-score method. This step was necessary because joint angles, angular velocities and current values have different numerical ranges. Without normalisation, the learning process would be dominated by variables with larger magnitudes, reducing the sensitivity of the model to smaller but diagnostically important changes. The same scaling parameters obtained from the training data were then used during validation and residual calculation, ensuring that the online model operated in the same numerical space as during training.

The adopted neural structure was a feedforward multilayer perceptron with one hidden layer of 15 neurons and ReLU activation. This architecture was selected as a compromise between approximation capability and computational simplicity. A larger network could fit the training data more closely but would increase the risk of overfitting to a single trajectory or to noise in the current signal. In contrast, a compact MLP is sufficient to model the smooth nonlinear relationship between robot configuration, joint velocity and nominal current demand during the repeatable figure-eight motion. Regularisation was applied to improve generalization and to prevent the model from learning high-frequency fluctuations as if they were deterministic physical effects.

The model was trained only on data representing nominal operation of the robot. This is important for anomaly detection. The reference model should describe the expected healthy state, so that deviations caused by external resistance, payload loss or increased friction remain visible in the residual. If faulty data were included in the training set without labels, the model could learn the anomaly as normal behaviour and reduce diagnostic sensitivity. The validation therefore focused on the ability of the network to reproduce the main current envelope under healthy conditions, not on minimizing every local oscillation.

The output layer generated the predicted current values for the robot joints. These predicted currents formed the reference signal used later in residual analysis. The residual was then calculated as the difference between measured and predicted current, as described in Section 2.3. This approach makes the neural model directly compatible with the physics-based interpretation of faults: an increase in residual indicates additional torque demand, while a decrease indicates unloading or loss of expected payload.

Figure 8 compares measured current signals for joints J1-J6 with the Digital Twin prediction. The agreement of the main signal envelope confirms that the reference model captures the dominant components of current demand caused by gravity, motion direction and friction. The prediction is not expected to reproduce every high-frequency fluctuation, because such components are partly related to drive electronics, PWM-based current control and closed-loop regulation of PMSM motors. This distinction is beneficial for condition monitoring. The model follows repeatable physical behaviour, while non-repeatable or persistent deviations remain visible as residuals.

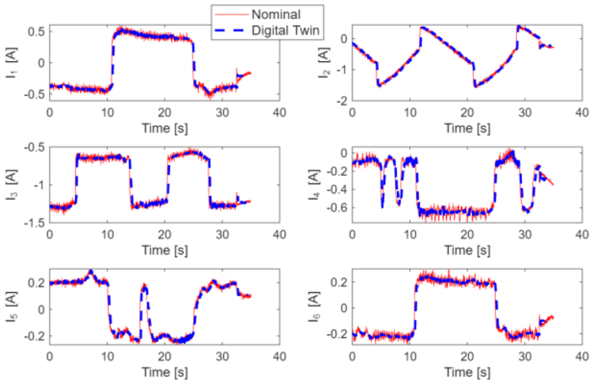

Fig. 8. Comparison of the measured motor currents for joints J1–J6 with the Digital Twin predictions under nominal conditions

To quantitatively verify the Digital Twin model prior to introducing simulated faults, the fidelity of the nominal current prediction was evaluated. Table 3 summarizes the performance metrics, including Root Mean Square Error (RMSE), Mean Absolute Error (MAE), and Coefficient of Determination (R^2), computed for the current residuals of all joints during nominal operation.

Table 3. Fidelity metrics of Digital Twin to robot current measurements for joints J1–J6

Metric	Joints					
	J1	J2	J3	J4	J5	J6
RMSE	0.036	0.041	0.032	0.046	0.023	0.025
MAE	0.029	0.033	0.024	0.035	0.015	0.019
R^2	0.991	0.994	0.989	0.972	0.992	0.987

In addition to model signal fidelity, the computational performance of the Digital Twin was assessed to ensure its suitability for online monitoring. The computational latency, defined as the time required for the virtual environment to process a single kinematic state from the 500 Hz RTDE data stream, remains on the order of fractions of a second. Although such latency is not critical for predictive diagnostics, it is nevertheless essential to account for it when calculating the residual signals. Furthermore, the synchronization jitter between the physical controller timestamps and the model's simulation steps was found to be negligible. While this slight processing delay means that the Digital Twin operates in a near real-time (pseudo-real-time) regime rather than strict hard real-time, it is fully sufficient for the purposes of condition monitoring, predictive maintenance, and early anomaly detection, where microsecond-level reactions are not required.

The small high-frequency oscillations visible in Fig. 8 should therefore not be interpreted as mechanical damage. They are present even under nominal conditions and are characteristic of the drive-control system.

4. EXPERIMENTAL INVESTIGATIONS

4.1. Definition of validation scenarios and residual evaluation

All experimental scenarios used the same figure-eight trajectory to keep the kinematic excitation comparable between tests. This trajectory produces alternating gravity loads and simultaneous motion of several joints, which makes it suitable for evaluating whether the residual signal is related to a real disturbance rather than to a trivial single-axis effect. The nominal run was used as the baseline, while disturbed runs were compared against the Digital Twin prediction under the same motion conditions.

The residual signal was evaluated in three complementary ways. First, its amplitude was used to determine whether the measured current departed from the healthy reference. Second, the sign of the residual was analysed because positive residuals indicate increased torque demand, whereas negative residuals indicate unloading or loss of expected payload. Third, the distribution of residuals across joints was considered, since a local mechanical disturbance should affect the directly loaded axis more strongly than the remaining joints. This interpretation prepares the analysis of Fig. 9-Fig. 12, where position trajectories, measured currents and residuals are used to distinguish external resistance from payload loss.

To evaluate the statistical repeatability of the experimental setup, the baseline figure-eight trajectory was executed across 10 consecutive cycles under nominal operating conditions. The standard deviation of the Root Mean Square (RMS) motor currents for each joint remained below 2% of the mean nominal values, indicating high consistency in both the mechatronic drive response and the RTDE communication layer. To ensure the robustness of the diagnostic system, the anomaly detection thresholds for each joint were defined using a three-sigma (3-sigma) safety margin above the maximum nominal Mean Absolute Error (MAE) listed in Table 3. Under the J5 resistance scenario, the current residuals exceeded these thresholds by an order of magnitude, ensuring a clear statistical separation between normal operating noise and mechanical degradation.

4.2. External resistance and mechanical anomaly simulation

Early mechanical degradation was simulated by controlled external resistance applied during the figure-eight motion. This experiment represents an increase in motion resistance that may be associated with lubrication degradation, bearing seizure, local friction growth or incipient gearbox damage. Figure 9 compares the joint-angle waveforms under nominal conditions and under external resistance. The similarity of the position trajectories indicates that the robot controller compensates for the disturbance and maintains motion, which explains why position monitoring alone is insufficient for early diagnosis.

Figure 10 presents the motor-current waveforms for axes J1-J6 under the same conditions. The current response shows a visible increase in demand during the disturbed motion. This confirms that current signals are more diagnostically informative than position signals when the controller hides the mechanical anomaly through feedback compensation.

Figure 11 shows the current residuals. The residual peaks identify the time intervals and axes most affected by the induced resistance. In the J5 resistance scenario, the largest relative deviations occur in the wrist axis because wrist motors operate with lower nominal torques; even moderate external forces therefore produce a large relative change in current. This supports local fault isolation but also indicates that residual thresholds should be joint-specific.

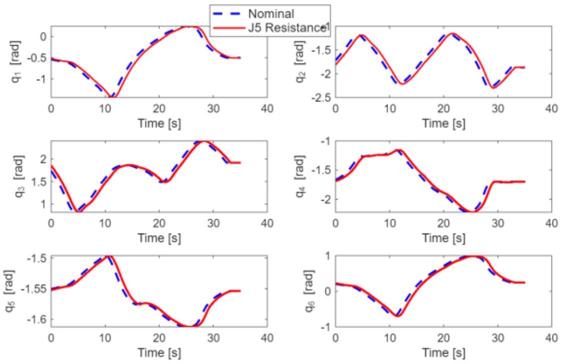

Fig. 9. Joint angle trajectories for axes J1–J6 under nominal conditions and in the presence of external resistance on J5

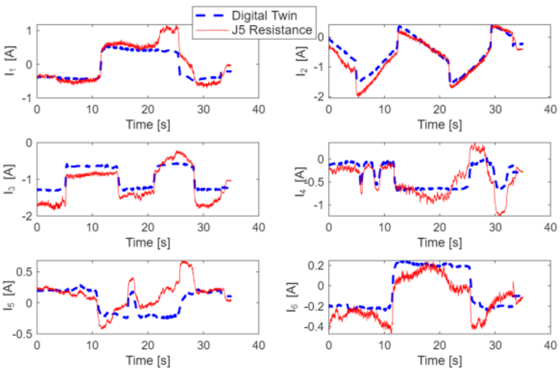

Fig. 10. Measured motor current waveforms for axes J1–J6 under nominal conditions and in the presence of external resistance on J5

For quantitative comparison with the nominal state, performance metrics were calculated for the J5 resistance scenario. Table 4 summarizes these metrics, including Root Mean Square Error (RMSE) and Mean Absolute Error (MAE), for the current residuals.

The residual metrics RMSE and MAE increased by approximately one order of magnitude compared to the noise level of the Digital Twin presented in Table 3, clearly indicating the presence of an anomaly.

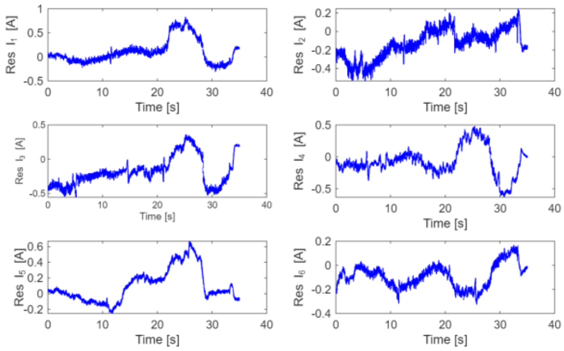

Fig. 11. Motor current residuals for axes J1–J6 under external resistance on J5

Table 4. Performance metrics for current residuals in joints J1–J6 under external resistance on J5

Metric	Joints					
	J1	J2	J3	J4	J5	J6
RMSE	0.268	0.205	0.276	0.238	0.231	0.132
MAE	0.183	0.162	0.250	0.189	0.167	0.111

However, identifying the exact joint responsible for the disturbance remains challenging due to dynamic coupling within the serial manipulator. Since friction is closely related to the velocity at a given joint, a key feature for fault localization is the correlation between the current residual and the angular velocity of each joint. Table 5 presents this cross-correlation matrix.

Table 5. Cross-correlation coefficients between current residuals and joint angular velocities (J5 resistance scenario)

		Angular Velocity					
		J1	J2	J3	J4	J5	J6
Current Residual	J1	0.30	-0.38	0.48	-0.13	-0.29	0.30
	J2	0.23	0.18	-0.01	-0.31	-0.13	0.23
	J3	0.23	-0.50	0.60	-0.13	-0.23	0.23
	J4	0.21	-0.56	0.57	0.03	-0.29	0.21
	J5	0.20	-0.19	0.21	-0.05	-0.04	0.20
	J6	-0.26	0.51	-0.60	0.08	0.42	-0.26

An evaluation of the results reveals that, counterintuitively, the matrix that the highest correlation coefficient does not occur at the directly affected joint—the correlation between the J5 residual and J5 velocity is negligible (-0.04). Instead, the highest correlation is observed at the proximal joint J3 (reaching approx. 0.60). This indicates that the robot controller utilizes the more powerful proximal joints to compensate for the distal resistance to maintain the programmed end-effector trajectory. This cross-correlation effect effectively illustrates why single-axis current monitoring is sufficient for anomaly detection, but insufficient for exact fault isolation without advanced multi-variable pattern recognition.

4.3. Payload-loss scenario

The second validation scenario was payload loss, corresponding to the release of a 0.5 kg object by the vacuum gripper. Figure 12 shows the total current consumption, defined as the sum of the absolute values of all six joint currents, for nominal motion and two payload-loss events.

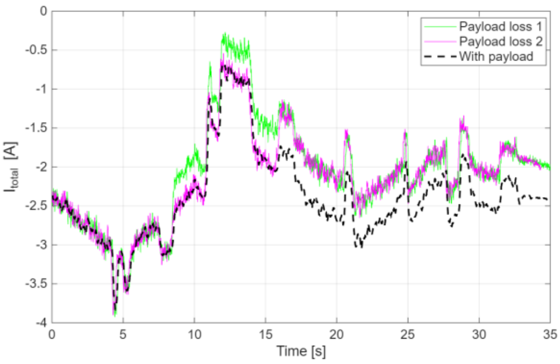

Fig. 12. Comparison of the total current consumption under nominal conditions and during 0.5 kg payload-loss events occurring at two different time instants

The presented time histories of the total current consumption I_{total} clearly differentiate the nominal operating condition from payload-loss scenarios. Under nominal conditions, when the gripper carries a 0.5 kg payload, the signal reaches the highest absolute values, reflecting the increased torque demand required to compensate for the mass of the transported medium. In both payload-loss scenarios caused by the vacuum gripper, a rapid step-like shift of the waveform toward zero is observed, amounting to approximately 0.5–0.8 A, which corresponds to a sudden reduction in the global energetic cost of executing the trajectory. An analysis of the time axis indicates that the first payload-loss event occurs at approximately t ≈ 8.5 s, while the second event takes place around t ≈ 16 s.

To visually illustrate transient behaviour, the joint-specific currents during the two payload-loss events are plotted in Figure 13.

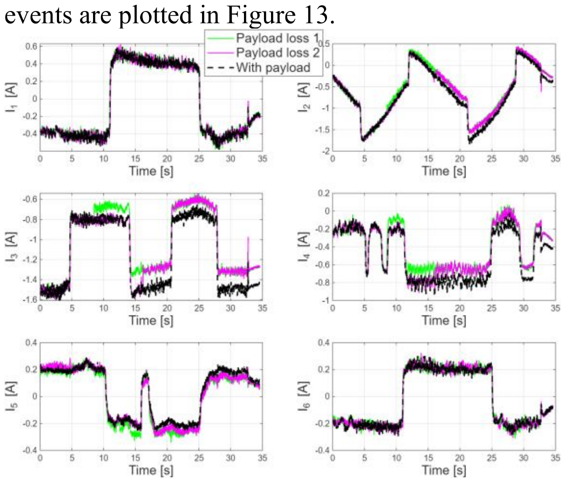

Fig. 13. Comparison of joint motor currents J1-J6 under nominal conditions and during 0.5 kg payload-loss events

Within the Digital Twin architecture, this phenomenon generates a characteristic negative residual signature, because the virtual model continues to estimate joint torques for a payload that is no longer physically present. Such a signal response provides a key criterion for unambiguous separation of process faults, such as payload loss, from mechanical anomalies including collisions or increased motion resistance, which instead lead to an increase rather than a decrease in current demand.

4.4. Advantages and Limitations

The developed current-residual-based Digital Twin observer offers several distinct advantages over traditional robot condition monitoring systems. Primarily, it enables sensorless implementation. Unlike vibration-based diagnostics that require external accelerometers, our method utilizes proprioceptive signals of encoder angles and motor currents available via the controller RTDE interface. This eliminates additional hardware cost, wiring complexity, and potential failure points, which are crucial for maintaining the safety certification of collaborative robots. Furthermore, the methodology provides joint-specific residual signals. While the robot built-in six-axis force-torque sensor can detect external collisions or payload loss at the end-effector, it cannot monitor individual internal joints. The proposed joint-specific residual vector $R(t)$ helps address this by providing individual current residuals for each drive axis.

However, certain limitations of this methodology must be noted. One major challenge involves bandwidth constraints. Motor current signals are inherently filtered by the mechanical inertia of the drive modules and the closed-loop current control of the PMSM controllers. Consequently, high-frequency structural faults such as early-stage bearing outer-race pitting are difficult to detect using currents alone, whereas dedicated high-frequency vibration sensors would easily capture them. Another limitation is friction dependency, since viscous friction is temperature dependent. Without active thermal calibration, a cold startup of the robot can generate false positive residuals that resemble mechanical degradation.

5. CONCLUSIONS

This paper presented the implementation and experimental validation of a Digital Twin framework for sensorless condition monitoring of a UR3e collaborative robot. By combining RTDE-based data acquisition with a calibrated virtual reference model, the proposed system successfully utilizes motor-current residuals to detect anomalies. The results confirm that current residuals can reveal mechanical and process disturbances that are typically masked in position trajectories due to the controller's active kinematic compensation.

The experimental scenarios validated the system's ability to distinguish between two distinct classes of events. External mechanical resistance resulted in positive residuals, indicating an increased torque demand. Conversely, process faults such as payload loss produced a characteristic negative residual signature due to a sudden reduction in the expected load. This directional interpretation of residuals provides a robust criterion for separating mechanical anomalies from process errors. Furthermore, the approach aligns with the ISO 23247 reference architecture, demonstrating how Digital Twin-based monitoring can effectively complement standard, collision-oriented safety systems by acting as an early-stage diagnostic layer.

While the proposed framework achieves highly reliable early fault detection, several limitations of this study must be addressed. First, the experimental validation was performed on a single robotic platform (Universal Robots UR3e). Manipulators from other manufacturers or those with different joint architectures (e.g., using RV reducers instead of harmonic drives) may exhibit different residual characteristics. Second, the simulated fault scenarios were limited to a step-like payload loss, and a localized friction increase on joint J5. Real-world mechanical degradation, such as gear wear or bearing wear, typically develops gradually and may affect multiple joints simultaneously. Third, the experiments were conducted in a controlled laboratory environment. Deploying the system in an actual industrial facility introduces additional disturbances, such as ambient vibrations, electromagnetic interference on current sensors, and variable duty cycles, which require further verification.

Therefore, a critical path for future work is integrating advanced multivariable pattern recognition and machine learning classifiers, or domain adaptation networks, to decouple dynamic effects and transition to precise fault isolation. Future developments will focus on two key directions. First, physics-informed machine learning will be used, implementing classifiers such as Random Forests, Support Vector Machines, or 1D Convolutional Neural Networks trained on features like cross-correlation and RMS residual energy to automate fault isolation. Second, the Digital Twin methodology will be validated by larger industrial manipulators using Rotate Vector reducers to evaluate signature scalability.

Source of funding: *The presented research was funded with grant No.3584/183/P (DBUPB/2023/011) for education allocated by the Ministry of Science and Higher Education of the Republic of Poland.*

Author contributions: *research concept and design, I.K.; Collection and/or assembly of data, G.S.; Data analysis and interpretation, I.K., G.S.; Writing the article, I.K., G.S.; Critical revision of the article, I.K.; Final approval of the article, I.K.*

Declaration of competing interest: *The authors declare that they have no known competing financial interests or personal relationships that could have appeared to influence the work reported in this paper.*

REFERENCES

1. Cheng L, Gao H, Sun W, Chen C, Xu X. An integrated method for predictive state assessment and path planning for inspection robots in island-based unmanned substations. Eksploatacja i Niezawodność – Maintenance and Reliability. 2025;27(4):16. https://doi.org/10.17531/ein/203994.
2. International Organization for Standardization. ISO 10218-1:2025 Robotics - Safety requirements - Part 1: Industrial robots. Geneva: ISO; 2025.
3. International Organization for Standardization. ISO/TS 15066:2016 Robots and robotic devices - Collaborative robots. Geneva: ISO; 2016.
4. Rumin P, Kotowicz J, Zastawna-Rumin A. Predictive maintenance of belt conveyor idlers based on measurements, analytical calculations and decision-making algorithms. Eksploatacja i Niezawodność – Maintenance and Reliability. 2025;27(4):6. https://doi.org/10.17531/ein/202096.
5. Grieves M, Vickers J. Digital Twin: Mitigating unpredictable, undesirable emergent behavior in complex systems. In: Kahlen FJ, Flumerfelt S, Alves A, editors. Transdisciplinary perspectives on complex systems. Cham: Springer; 2016. https://doi.org/10.1007/978-3-319-38756-7_4.
6. Mazumder A, Sahed M, Tasneem Z, Das P, Badal F, Ali M, et al. Towards next generation digital twin in robotics: Trends, scopes, challenges, and future. Heliyon. 2023;9(2):e13359. https://doi.org/10.1016/j.heliyon.2023.e13359.
7. Geronel RS, Silva MM. Digital twins in robotic applications. In: Avancos recentes em Ciencias da Engenharia: volume 1. Sao Carlos: Universidade de Sao Paulo; 2025. Available from: https://www.researchgate.net/publication/391159892_Digital_twins_in_robotic_applications.
8. International Organization for Standardization. ISO 23247-2:2021 Automation systems and integration - Digital twin framework for manufacturing - Part 2: Reference architecture. Geneva: ISO; 2021.
9. International Organization for Standardization. ISO/IEC 30141:2024 Internet of Things (IoT) - Reference architecture. Geneva: ISO; 2024.
10. Mo F, Rehman HU, Chaplin JC, Sanderson D, Ratchev S. Digital twin-based self-learning decision-making framework for industrial robots in manufacturing. Int J Adv Manuf Technol. 2025;139:221-240. https://doi.org/10.1007/s00170-025-15844-w.
11. Zhang Y, Gao P, Wang Z, He Q. Research on status monitoring and positioning compensation system for digital twin of parallel robots. Sci Rep. 2025;15:7432. https://doi.org/10.1038/s41598-025-91892-2.
12. Ayankoso S, Kaigom E, Louadah H, Faham H, Gu F, Ball A. A hybrid digital twin scheme for the condition monitoring of industrial collaborative robots. Procedia Comput Sci. 2024;232:1099-1108. https://doi.org/10.1016/j.procs.2024.01.108.
13. Ouarhlent S, Terki N, Hamiane M, Dahmani H. Fault detection in robots based on discrete wavelet transformation and eigenvalue of energy.

Diagnostyka. 2023;24(4):2023407. https://doi.org/10.29354/diag/174124.
14. Sabry AH, Ungku Amirulddin UAB. A review on fault detection and diagnosis of industrial robots and multi-axis machines. Results Eng. 2024;23:102397. https://doi.org/10.1016/j.rineng.2024.102397.
15. Zhang Y, Wu J, Gao B, Xia L, Lu C, Wang H, et al. Fault Types and Diagnostic Methods of Manipulator Robots: A Review. Sensors. 2025;25(6):1716. https://doi.org/10.3390/s25061716.
16. Khan Z, Nasir A, Mekid S. Fault-tolerant control strategies for industrial robots: state of the art and future perspective on AI-based fault management. Artif Intell Rev. 2025;58(11):362. https://doi.org/10.1007/s10462-025-11327-2.
17. Zhang G, Tao Y, Wang J, Feng K, Han X. A Motor current signal-based fault diagnosis method for harmonic drive of industrial robot under time-varying speed conditions. IEEE Trans Instrum Meas 2025; 74:1-10. https://doi.org/10.1109/TIM.2025.3529564.
18. Hsieh N, Yu T. Fault detection in harmonic drive using multi-sensor data fusion and gravitational search algorithm. Machines. 2024;12(12):831. https://doi.org/10.3390/machines12120831.
19. Qiao Y, Wang H, Cao J, Lei Y. Sound-vibration spectrogram fusion method for diagnosis of RV reducers in industrial robots. Mech Syst Signal Process. 2024;214:111411. https://doi.org/10.1016/j.ymssp.2024.111411.
20. Elahi MU, Raouf I, Khalid S, Ahmad F, Kim HS. Transfer Learning-Based Health Monitoring of Robotic Rotate Vector Reducer Under Variable Working Conditions. Machines. 2025;13(1):60. https://doi.org/10.3390/machines13010060.
21. Ren G, Wang Z, Liu X, Song F. Remaining useful life prediction of industrial robot RV reducer with multiple deep networks and multicore support vector data description. J Mech Sci Technol. 2024;38(8): 4037-4051. https://doi.org/10.1007/s12206-024-0703-y.
22. Liu W, Han B, Zheng A, Zheng Z, Chen S, Jia S. Fault diagnosis of reducers based on digital twins and deep learning. Sci Rep. 2024;14:24406. https://doi.org/10.1038/s41598-024-75112-x.
23. Zhang W, Zhang T, Cui G, Pan Y. Dynamics analysis and deep learning-based fault diagnosis of defective rolling element bearing on the multi-joint robot. Machines. 2022;10(12):1215. https://doi.org/10.3390/machines10121215.
24. Rohan A, Raouf I, Kim HS. Rotate Vector (RV) Reducer fault detection and diagnosis system: towards component level prognostics and health management (PHM). Sensors. 2020;20(23):6845. https://doi.org/10.3390/s20236845.
25. Tu Z, Gao L, Wu X, Liu Y, Zhao Z. Rotate vector reducer fault diagnosis model based on EEMD-MPA-KELM. Appl Sci. 2023;13(7):4476. https://doi.org/10.3390/app13074476.
26. Jaber AA, Bicker R. Fault diagnosis of industrial robot bearings based on discrete wavelet transform and artificial neural network. Int J Progn Health Manag. 2016;7(2). https://doi.org/10.36001/ijphm.2016.v7i2.2365.
27. Jaber AA, Bicker R. Industrial robot backlash fault diagnosis based on discrete wavelet transform and artificial neural network. Am J Mech Eng. 2016; 4(1):21-31. https://doi.org/10.12691/ajme-4-1-4.
28. Alobaidy MAA, Abdul-Jabbar JM, Aly M, Hassanpour R. Real time fault diagnosis in industrial robotics using discrete and slantlet wavelet transformations. Sci Rep. 2025;15:34145. https://doi.org/10.1038/s41598-025-09272-9.
29. Chen Z, Fu H, Zeng Z. A domain adaptation neural network for digital twin-supported fault diagnosis. In: International Conference on Control, Automation and Diagnosis (ICCAD). Piscataway: IEEE. 2025:1-6. https://doi.org/10.1109/ICCAD64771.2025.11099349.
30. Ben Hnaien I, Gascard E, Simeu-Abazi Z, Dhouibi H. Fault diagnosis of industrial robots using a digital twin and GRU-Based Deep Learning. In: Proceedings of the 22nd International Conference on Informatics in Control, Automation and Robotics. Setubal: SCITEPRESS. 2025:487-494. https://doi.org/10.5220/0013705600003982.
31. Universal Robots. e-Series User Manual and RTDE Client Interface documentation. Odense: Universal Robots; 2024. Available from: https://docs.universal-robots.com.
32. Lindvig AP, Iturrate I, Kindler U, Sloth C. ur_rtde: An interface for controlling universal robots (UR) using the Real-Time Data Exchange (RTDE). In: 2025 IEEE/SICE International Symposium on System Integration (SII). Piscataway: IEEE; 2025: 1118-1123. https://doi.org/10.1109/SII59315.2025.10871000.
33. International Organization for Standardization. ISO 9283:1998 Manipulating industrial robots - Performance criteria and related test methods. Geneva: ISO; 1998.
34. Lynch KM, Park FC. Modern robotics: Mechanics, planning, and control. Cambridge: Cambridge University Press; 2017
35. Bittencourt AC, Axelsson P, Jung Y, Brogardh T. Modeling and identification of wear in a robot joint under temperature uncertainties. IFAC Proc Vol 2011;44(1):10293-10299. https://doi.org/10.3182/20110828-6-IT-1002.01078.
36. MathWorks. Simscape Multibody Documentation. Natick: The MathWorks, Inc.; 2024. Available from: https://www.mathworks.com/help/physmod/sm/.

Iwona KOMORSKA, DSc., DEng. – Associate Professor at Radom University. Her current research interests include mechatronics, technical diagnostics, data mining, machine learning, signal processing, modelling & simulation.
e-mail: iwona.komorska@uthrad.pl

Grzegorz STEFANIAK, Eng., is a graduate of Robotics and Process Automation at Casimir Pulaski Radom University. His research interests include collaborative robotics, digital twins, industrial automation and CNC manufacturing.
e-mail: grzegorzstefaniak@vp.pl